GA–A26778

THE INFLUENCE OF THREE-DIMENSIONAL STOCHASTIC MAGNETIC BOUNDARIES ON PLASMA EDGE TRANSPORT AND THE RESULTING PLASMA WALL INTERACTION

by
O. SCHMITZ, T.E. EVANS, J. BOEDO, M.E. FENSTERMACHER,
M. JAKUBOWSKI, R. LAENGNER, A. McLEAN, D. ORLOV, H. REIMERDES,
J.G. WATKINS, N.H. BROOKS, C.L. LASNIER, H. FRERICHS,
D. REITER, U. SAMM, H. STOSCHUS, E.A. UNTERBERG
AND THE DIII-D AND TEXTOR TEAMS

JULY 2010

GENERAL ATOMICS

DISCLAIMER

GA–A26778

THE INFLUENCE OF THREE-DIMENSIONAL STOCHASTIC MAGNETIC BOUNDARIES ON PLASMA EDGE TRANSPORT AND THE RESULTING PLASMA WALL INTERACTION

by
O. SCHMITZ,[*] T.E. EVANS, J. BOEDO,[†] M.E. FENSTERMACHER,[‡]
M. JAKUBOWSKI,[¶] R. LAENGNER,[*] A. McLEAN,[§] D. ORLOV,[†]
H. REIMERDES,[#] J.G. WATKINS,[◊] N.H. BROOKS, C.L. LASNIER,[‡]
H. FRERICHS,[*] D. REITER,[*] U. SAMM,[*] H. STOSCHUS,[*]
E.A. UNTERBERG,[§] and THE DIII-D and TEXTOR TEAMS

This is a preprint of a paper to be presented at the Nineteenth International Conference on Plasma Surface Interactions, May 24-28, 2010, in San Diego, California, and to be published in the *Proceedings.*

[*]Forschungszentrum Juelich, Association EURATOM-FZJ, Juelich, Germany.
[†]University of California-San Diego, La Jolla, California.
[‡]Lawrence Livermore National Laboratory, Livermore, California.
[¶]Max-Planck-Institut für Plasmaphysik, Greifswald, Germany.
[§]Oak Ridge National Laboratory, Oak Ridge, Tennessee.
[#]Columbia University, New York, New York.
[◊]Sandia National Laboratory, Albuquerque, New Mexico.

Work supported in part by
the U.S. Department of Energy
under DE-FC02-04ER54698, DE-FG02-07ER54917, DE-AC52-07NA27344,
DE-FG02-89ER53297, DE-AC05-00OR22725, and DE-AC04-94AL85000

GENERAL ATOMICS PROJECT 30200
JULY 2010

GENERAL ATOMICS

ABSTRACT

The three-dimensional features of the magnetic topology induced by edge resonant magnetic perturbation fields are discussed comparing TEXTOR and DIII-D. We show that the scrape-off layer (SOL) profiles and decay lengths depend on the RMP spectral properties indicating modification of SOL transport by the 3D stochastic boundary because the particle and heat efflux is channelled along the perturbed field lines into a completely re-arranged, 3D divertor footprint. The measured divertor heat and particle fluxes at DIII-D match the vacuum modelled magnetic footprint in L-mode while in H-mode it exceeds the modelled footprint width by 10-20%. Initial first quantification of the net-erosion within the 3D footprint shows in L-mode a 40% decrease of the chemical erosion and evidence for a comparably small 5-15% increase in physical sputtering. Extrapolation of these findings to ITER by modelling of the magnetic footprint for the actual ELM control coils shows a similar footprint topology as found at DIII-D during RMP ELM suppression. However, the open field lines escape the CFC covered ITER divertor area and hit the Tungsten divertor domain.

I. INTRODUCTION

The control and optimization of the plasma wall interaction by externally applied magnetic perturbation fields with a field line pitch angle alignment on selected rational surfaces in the plasma edge is an attractive technique for future fusion devices. At DIII-D it was demonstrated that edge resonant magnetic perturbation (RMP) fields with a dominant toroidal mode number $n = 3$ can be used to completely eliminate large type-I edge localized modes (ELMs) [1,2], an important task to avoid transient, impulsive heat and particle loads at ITER and preserve the integrity of the ITER divertor and plasma facing components (PFCs) of the main chamber [3]. At JET mitigation of type-I ELMs was demonstrated [4] with low toroidal mode number $n = 1,2$ fields applied from large aspect ratio external coils. Subsequent efforts on other devices like the spherical tokamaks MAST [5] and NSTX [6] have extended the physics data base for ELM control by RMP and this world wide effort is accompanied by basic research on TEXTOR [7] following up many aspects of predecessor devices in RMP research like JFT-2M [8], Compass-D [9], JT-60 [10] and Tore Supra [11] for instance. The detailed characteristics of the plasma response to external RMP perturbation fields are still an unresolved and intensively discussed issue, however, on all devices coherent evidence is found for the formation of a three-dimensional (3D) plasma boundary with at least a thin layer of open, stochastic field lines. Due to the external RMP field the axisymmetry of the tokamak is broken and the plasma boundary is re-arranged into a 3D topology determined by the spectral properties of the external field. In particular, field lines in the plasma edge get connected to the PFCs of the main chamber and the divertor surface forming a 3D magnetic footprint, therefore causing the plasma surface interaction to be an inherently 3D physics task. In this contribution, experimental results for these facts will be discussed from TEXTOR [12] as an example for a circular, high field side limited plasma device, mostly operating in L-mode and DIII-D [13] as an example for a poloidally diverted L- and H-mode plasma with the capability to generate high triangularity ITER similar shaped (ISS) plasmas at ITER relevant low pedestal electron collisionality $\nu_e^* < 0.1$ and complete ELM suppression [14]. Basic concepts are introduced on the example of TEXTOR and applied for analysis of the plasma wall interaction in ISS plasmas at DIII-D including ELM suppression. The extrapolation of these findings is discussed based on modelling of the perturbed magnetic footprint for the latest ELM control coil configuration at ITER.

II. STRUCTURE OF THE STOCHASTIC MAGNETIC EDGE LAYERS AT TEXTOR AND DIII-D

We discuss in this paper the effect of resonant magnetic perturbation fields where the resonance is defined by the alignment of the external field harmonics with the magnetic field line pitch angle on selected rational surfaces in the plasma edge. Resonances with ideal [15] or resistive MHD [16] modes in the plasma are not considered within the RMP terminology used. The particular aspect of the RMP fields as applied at TEXTOR and DIII-D for formation of a 3D stochastic boundary is a rich spectrum of poloidal (m) and toroidal (n) harmonics of $m = 8\text{-}14,\ n = 4,3,2$ at TEXTOR and $m = 3\text{-}12,\ n = 3,2,1$ at DIII-D which have the potential to induce a wide variety of resonant Poincaré type island chains. The magnetic topology induced by this kind of RMP fields is described for example in [17] for TEXTOR and [18] in comparison to DIII-D. The theoretical background is surveyed in [19] and references therein. To illuminate the perturbed magnetic topology at TEXTOR and DIII-D, we calculate the magnetic field line connection length L_c by field line tracing in the so-called vacuum paradigm, i.e. the linear superposition of the external field onto an axisymmetric 2D plasma equilibrium. Figure 1 shows the L_c distribution in the stochastic layer illuminating the 3D boundary structure in circular limited plasma for the TEXTOR case [Fig. 1(a)] and for the poloidally-diverted case at DIII-D [Fig. 1(b)]. The resonant islands generated can overlap in case of sufficiently high spectral amplitudes on the resonant surfaces forming a stochastic layer and close to the edge a layer of short connection length field lines evolves with correlated magnetic field line trajectories. These field lines form at TEXTOR [20] and DIII-D [21] coherent magnetic flux bundles which channel the particle and heat efflux by direct parallel transport towards the divertor surface elements. These so-called laminar flux tubes form the helical and highly 3D scrape-off layer of RMP induced stochastic boundaries and they are embedded into stochastic field lines which represent the interface to the confined region in the plasma core. Very similar magnetic layer topologies were also found in helical devices [22] and stellarator experiments [23] showing that the topological properties introduced here are generic for application of field aligned RMP fields.

The magnetic footprint which determines the interaction of the stochastic layer induced transport and resulting plasma efflux with the wall is determined by a generic structure within the 3D boundary – the invariant manifolds of the resonant island chains themselves [24] and of the separatrix for the poloidal divertor case [18,19]. The separatrix in a poloidally diverted axisymmetric plasma is composed of field lines which

can be traced on trajectories forward and backward in toroidal direction. The X-point has a strong influence on these field lines, as a so-called hyperbolic fixed point [17] which defines the separatrix and the last closed flux surface (LCFS). When the separatrix is perturbed by even small radial magnetic fields a new set of boundary conditions for the "equation of motions" of the field lines is defined, so-called invariant manifolds. The new field line trajectories cause direct short cuts from the plasma interior and the LCFS to the divertor target where they intersect in a helical pattern formed by the so-called homoclinic tangles [18,19,21] of the perturbed separatrix and determined by the poloidal and toroidal distribution of the radial perturbation field component. It is of fundamental importance to note that the separatrix perturbation and therefore the resulting shape of the magnetic divertor footprint is a non-resonant process [25] while the transport response within the interior stochastic layer filling the laminar flux tubes is a field line pitch resonant process and therefore dependent on RMP field penetration. However, plasma response currents modifying the RMP amplitudes inside the plasma cause additional radial field components which interact again with the separatrix. Therefore the separatrix is a fine sensor for the resulting perturbation field at the separatrix and comparison to magnetic footprint modelling can tell us how well vacuum magnetic field line tracing describes the newly established 3D boundary.

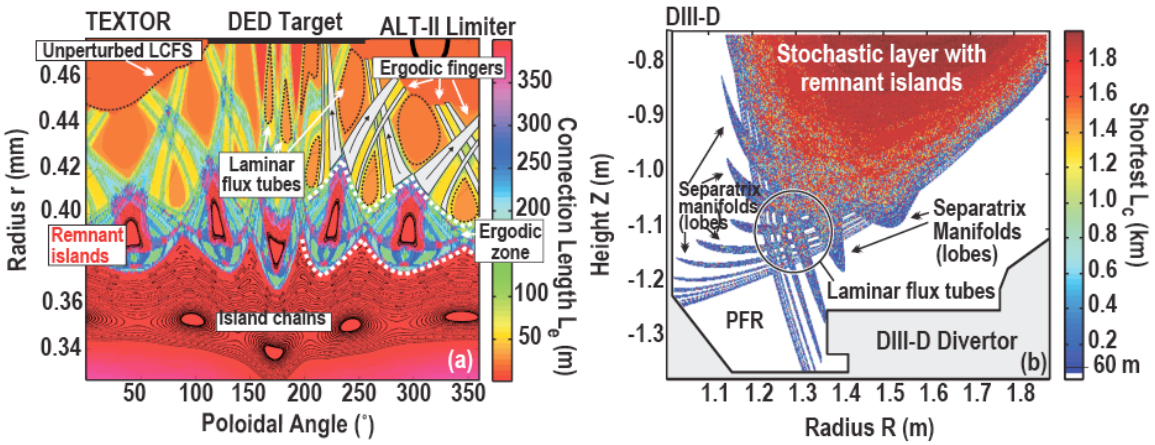

Fig. 1. Perturbed magnetic boundary layer as colour coded field line connection lengths plots for TEXTOR (left side) and DIII-D (right side).

III. PLASMA EDGE TRANSPORT AND SCRAPE-OFF LAYER PROFILES WITH RMPS

During ELM suppression in ISS plasmas at DIII-D with low $\nu_e^* < 0.1$, a resonant reduction of the electron pedestal pressure $p_e(r,t)$ was observed coherent to a pitch alignment dependence of the vacuum modelled stochastic layer width [26] with robust ELM suppression at the strongest p_e reduction spot. The same dependence of p_e in the plasma edge on the stochastic layer width was extracted from accompanying TEXTOR experiments suggesting in combination that open field lines in the edge connect to the target and are able to drive enhanced outward heat and particle fluxes. This concept was also found in recent results of 3D plasma fluid and kinetic neutral transport modelling with the EMC3-Eirene code for similar discharges [27]. One important question is to what extent this RMP induced transport affects the scrape-off layer (SOL) profile decay length and the resulting heat and particle fluxes to the divertor and PFCs. In Fig. 2, the dependence of the SOL profile shapes on the spectral properties of the RMP field at TEXTOR and DIII-D is shown.

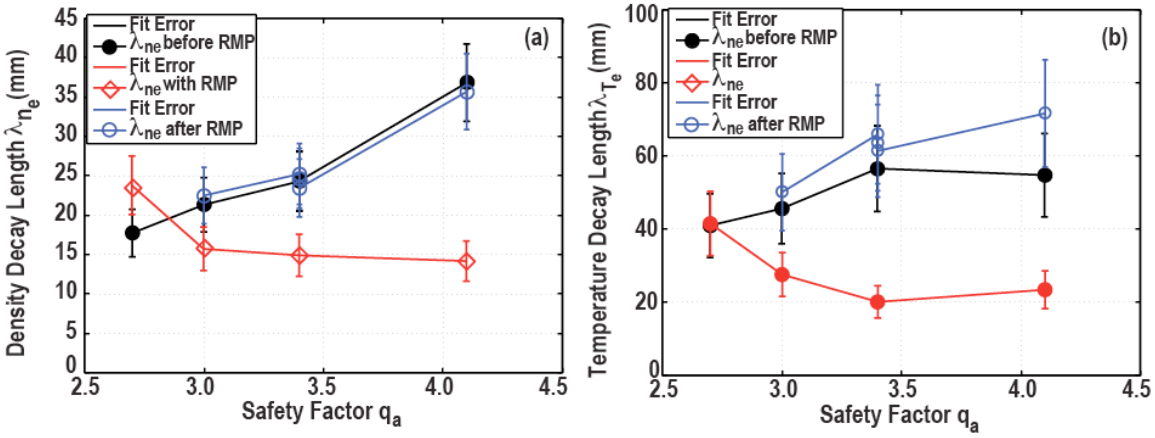

Fig. 2. Edge safety factor dependence of the scrape-off layer decay length (a) λ_{ne} and (b) λ_{Te} for the TEXTOR edge plasma with and with out RMP field applied.

For the TEXTOR case the local resonant amplitude was scanned using the edge safety factor q_a, i.e. by moving the resonant surfaces closer to the perturbation source. In Fig. 2(a), the electron density decay lengths λ_{ne} is shown as a function of q_a for a sequence of no-RMP discharges in comparison with those from RMP discharges. The RMP field applied was a m/n =12/4 dominant spectrum with a relative perturbation field B_r to toroidal field B_T of $B_r/B_T \sim 10^{-3}$, i.e. we used a spectrum and amplitude ratio similar to the one planned currently for ITER. Figure 2(b) shows for the same set of

discharges the electron temperature decay length λ_{Te}. This study proves a q_a resonant steepening of both n_e and T_e profiles when q_a is reduced. While for the no-RMP case a general flattening of both profiles with increasing q_a is observed, the profiles steepen considerably with the RMP field applied. This is caused by the formation of laminar flux tubes, which act as an efficient helical SOL with predominant parallel transport which governs the net-transport balance without any modification of cross field diffusion [20]. The flux tubes therefore channel effectively heat and particle fluxes towards the target at the high field side [20,28]. Here, these fluxes get compressed and deposited into thin helical stripes that are determined in width and location by the invariant manifolds of the outermost resonant island chain [24]. This proves that the potentially enhanced radial heat and particle flux from the stochastic boundary layer can be captured and effectively exhausted through the laminar zone of the stochastic layer as the new 3D SOL [20]. This was also found in the topologically comparable "edge surface layer" of LHD and proven to be capable for fine tuning of particle fuelling with improved impurity screening as well as maintaining stable detachment at LHD and W7-AS [22,23].

At DIII-D a similar trend as observed at TEXTOR was found investigating SOL profiles in high field side limited discharges at fixed edge safety factor q_{95} = 3.1 with the RMP field spectra as typically used for ELM suppression ($n = 3$ fields with $m = 4$-13) and a $n = 1$ dominated field ($m = 2$-5) on the level of the $n = 1$ error field of DIII-D. Figure 3 shows the gradient lengths L_n of the n_e profiles on the left and L_T of the T_e profiles on the right for two radial domains. First we study the profile region within $+/-2$ cm of the last closed flux surface (LCFS) shown as green and blue diamonds in Fig. 3 and second we analyze the SOL profiles for $dR_{sep} > 2$ cm distance from the separatrix shown with square markers in Fig. 3 We compare the gradient length for (a) a discharge with noRMP applied, (b) a discharge at low rotation with an injected power of 900 kW and (c) a discharge with the same injected power but a 50% increase of the tangential injection and therefore an increase of the toroidal rotation from 15 km/s at the edge to 30 km/s.

At low rotation we measure a steepening of the ne profile at the LCFS with a decrease of L_n from 8 cm to 4.5 cm when an $n = 3$ field is applied while L_n is marginally affected by the $n = 1$ field. In contrast the T_e profile flattens at LCFS with an increase of L_T from ~ 4.5 cm to 7 cm when the $n = 1$ field is applied and to 9 cm with $n = 3$ field. This reveals a strong impact of both RMP spectra on the electron temperature profile in the vicinity of the separatrix. In the SOL domain of the measured profiles we consistently measure at low rotation an increase of L_n and a decrease of L_T, which shows a decoupling of the effective net-transport characteristics in both profile regions. When the toroidal rotation is increased by a factor of 2, these effects get damped, i.e. all relative changes in between the RMP and noRMP phase for both dominant RMP toroidal modes are reduced in both profile domains. This indicates a dependence of the edge magnetic

topology and the net-radial plasma edge transport on the toroidal rotation as reported recently for fast rotating RMP fields at TEXTOR [30].

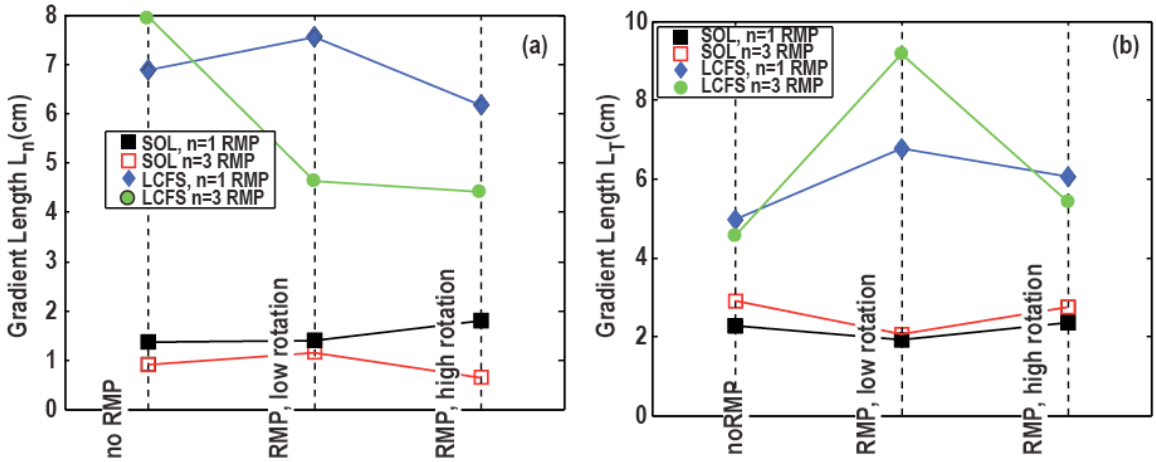

Fig. 3. Edge profile decay lengths with RMP at the last closed flux surface (LCFS) and in the scrape-off layer (SOL) of DIII-D. Depicted are gradient lengths for L-mode high field side limited plasmas for noRMP case, RMP case at low rotation (15 km/s in the edge) and higher rotation (30 km/s).

These characteristic SOL modifications show that the balance of radial efflux and parallel channelling of these fluxes towards the wall and divertor area have changed. These measurements are single space point measurements within the complex 3D boundary and as shown in [24,29,30] the impact of these findings on the eventual PFC and divertor heat and particle flux distribution is dependent on the poloidal and toroidal shape of the measured n_e and T_e fields. We therefore concentrate now on experimental results of heat and particle fluxes to the DIII-D divertor and compare them to the vacuum modelled magnetic topology in order to assess the consequences of the measured plasma edge and SOL profile changes.

IV. DIVERTOR PARTICLE AND HEAT FLUXES DUE TO THE RMP INDUCED 3D SEPARATRIX

The particle and heat fluxes exhausted by the open field lines in the stochastic edge are channelled towards the divertor target plates and deposited in a helically striated magnetic divertor footprint pattern [18,20,21,28]. The imprint of this magnetic footprint was observed reliably during application of RMP fields for ELM suppression at DIII-D. However, while at high pedestal electron collisionality ν_e^* the measured striation exceeds the one modelled by vacuum magnetic field line tracing by up to a factor of 3 [31], a fair agreement was found for ISS plasmas at low ν_e^*. In Fig. 4, a systematic assessment of this observation is presented. We compare the results of the correlation between the measured heat $q_{||}$ and particle fluxes $\Gamma_{||}$ (CII intensity is used as a proxy for the ion influx in an attached divertor where the carbon source depends predominantly on the physical sputtering yield) with the modelled magnetic footprint at the measurement location.

Figure 4(a) shows this comparison for an L-mode plasma with the outer divertor leg positioned on the lower outer shelf of DIII-D. With this arrangement all lobes evolving at the outer leg can be nicely observed. We plot the radial location at which a field line launched from the measurement location reaches on an electron mean free path length of λ_{ee} = 120 m as a metric for the magnetic topology connecting the measurement location with a position upstream along the field line inside of the plasma. For the L-mode [Fig. 4(a)] case we find a very good alignment of the heat and the particle flux with the magnetic topology and the location where the separatrix lobes strike the shelf at the outer strike line. This result suggests that the exhausted heat and particle fluxes are channelled along the open field lines by a direct parallel transport with low remaining cross field fluxes – otherwise the observed footprint pattern would be blurred and no striation would be visible [18,28]. The good match to the modelled topology shows that the 3D boundary for this plasma regime is well described by this modelling approach.

Figures 4(b) and 4(c) show the same assessment for ISS shaped H-mode plasmas at ν_e^* = 0.1 during complete ELM suppression by RMP. Again the striation of the heat and particle fluxes is observed and the number of stripes as well as the approximate location is in agreement with the vacuum modelling. However, in detail we observe a splitting which is consistently 10-20% wider than the one modelled. This could indicate plasma response currents which modify the local perturbation amplitude at the separatrix or it could be caused by uncertainties in the magnetic equilibrium, i.e. in the actual q_{95} value in particular. It was measured [18] that during ramping of q_{95} the separatrix lobes spiral

helically across the divertor target. Modification of the q_{95} profile by bootstrap currents in H-mode plasmas increases the uncertainty in the q_{95} value obtained by EFIT and therefore may cause the small deviation between the vacuum modelled footprint and the striated divertor heat and particle fluxes observed. Figure 7 in [18] shows that a small change of $\Delta q_{95} < 0.2$ is sufficient to shift the lobe location by $+/-5$ mm in the radial direction. Therefore we consider this as a fair agreement and the vacuum model is an applicable technique to describe the plasma boundary and the plasma surface interaction. Effort to include a plasma response in the modelling of the separatrix and the strike line striation is ongoing (see e.g. [32,33]) but complex due to the asymptotic behaviour of plasma current profiles at the separatrix.

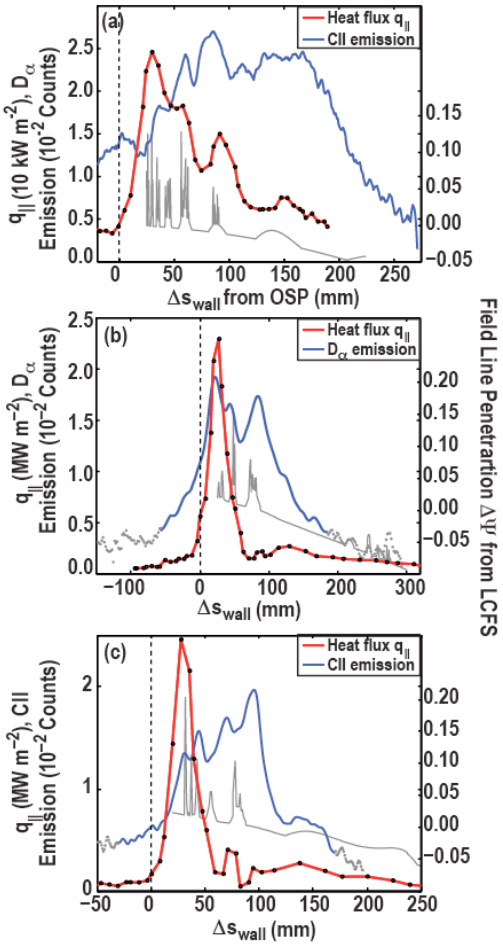

Fig. 4. Comparison of heat flux (red) and CII emission (λ = 514 nm, blue profile, used as measure for the ion influx) with the local field line penetration depth profile (grey) for (a) an L-mode discharge, (b) a discharge with ELM suppression but no strong T_e drop (see [18], here the blue curve represents the D_α emission (λ = 656.2 nm)) and (c) a discharge at the optimum resonant spot with thermal transport enhancement and robust ELM suppression (see [27]). The x-axis depicts the distance Δs_{wall} along the wall from the strike point.

Comparison of Fig. 4(b) with Fig. 4(c) highlights an interesting relation of pedestal parameters and the measured heat flux. As reported in [26], a q_{95} resonant enhancement of the thermal transport was observed yielding a resonant reduction of the pedestal electron pressure. Figure 4(b) shows a result with $q_{95} = 3.6$, i.e. at the boundary of the resonant window for ELM suppression. Here, no strong thermal loss was detected and therefore only a small heat flux into the outer separatrix lobes is measured. In contrast, in Fig. 4(c) taken at a $q_{95} = 3.45$ value with strong pedestal T_e reduction and potentially high thermal loss along the open field lines shows accordingly $\Delta q_{||} = 350\ \mathrm{kW/m^2}$ more heat flux density channelled into the second outer lobe.

These findings show in summary that (a) the vacuum modelled boundary is a feasible attempt to be used for studying the plasma wall interaction under impact of RMP fields for ELM suppression and (b) that there is a connection between the pedestal profiles observed and the measured heat and particle fluxes on the target. The details of this link are still matter of ongoing research, however, with this understanding we attempt to quantify the erosion properties in the 3D boundary induced.

V. EXPERIMENTAL CHARACTERIZATION OF CARBON EROSION INSIDE OF THE 3D SEPARATRIX LOBES

At DIII-D the Porous Plug Injector (PPI) [34] was developed as a module for the Divertor Material Evaluation System (DiMES) to measure the chemical carbon erosion yield Y_{chem}. The concept behind this technique is to inject a small but well-known hydrocarbon flux $\Gamma_{CH\ PPI}$ into the divertor region which is in the order of the intrinsic chemically eroded carbon influx ($10^{17}-10^{18}$ molecules s^{-1}). In combination with a local measurement of the deuterium ion influx Γ_{D+} this allows to use the ratio $\Gamma_{CH\ PPI}/\Gamma_{D+}$ together with the CH band emission at the PPI cap $\Phi_{CH\ PPI}$ and with the photon flux $\Phi_{CH\ ref}$ of a reference volume adjacent to the PPI cap to calculate $Y_{chem.} = (\Gamma_{CH\ PPI}/\Gamma_{D+})^{*}\ (\Phi_{CH\ ref}/\Phi_{CH\ PPI})$ (please see Ref. [34,35] and Eq. (2) in [35] for more details). This technique provides a mean for direct measurement of Y_{chem} without high-localized CH fluxes and the need to obtain exact photon efficiencies and assess all CH break-up chains as applied routinely at TEXTOR for example [36].

We analyse with this strategy an experiment in which the outer strike point was swept across the PPI cap with the $n = 3$ field applied as typically used during ELM suppression. As the acceptable heat influx to the PPI cap is limited to L-mode plasma levels, we performed this RMP experiment in a lower single null diverted L-mode plasma. The chemical erosion yield Y_{chem} is depicted in Fig. 5 in comparison to the relative increase of the CII emission in the PPI cap measurement volume relative to the reference volume. Five distinct phases are considered during the outer strike point sweep. We start with the PPI cap located in the SOL of the perturbed boundary and then move stepwise three lobes across the PPI cap such that the lobe is on the cap for the integration time of the MDS spectrometer used. We therefore get data where the local erosion properties are dominated by single separatrix lobes marked with different colours of the square markers in Fig. 5. At the end of the strike point sweep the PPI cap is located in the private flux region (PFR) of the perturbed boundary. We measure a reduction of the chemical erosion yield within the separatrix lobes and a reduction of the relatively higher CII emission in the PPI cap measurement volume. This means considering the difference between Y_{chem} and the CII emission as a quantity linked to the change of the physical sputtering, that inside of the lobes in general the carbon source is reduced but the fraction of the physical sputtering increases as Y_{chem} decreases. Inspection of the PPI cap in comparison to discharges without RMP application shows that the local re-deposition pattern observed in an axisymmetric boundary being aligned along the toroidal field direction is not visible anymore. Instead, the colometric distribution on the PPI cap exposed in the RMP

boundary indicates direct local re-deposition as the ion influx [37] inside of the lobes is higher than the local axisymmetric values and therefore faster ionisation of the CH molecules more prompt re-deposition close to the erosion location is likely. However, it is important to note that this is one local measurement in a complex 3D boundary only and matter of more detailed study with full 3D codes capable to handle both sides of the problem (a) the plasma fluid modelling in a 3D boundary and (b) the surface interaction including a dynamical surface layer model.

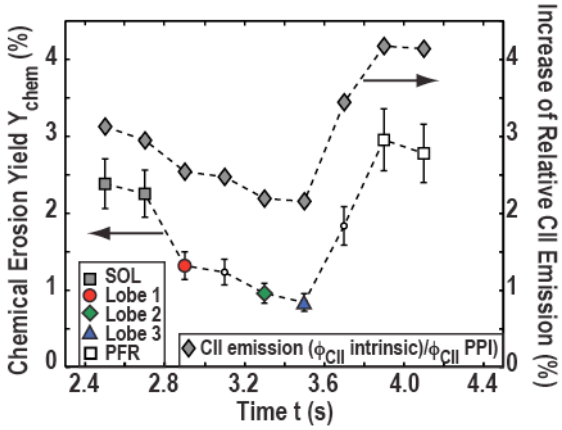

Fig. 5. Chemical erosion yield and relative increase of the CII emission at the location of the PPI cap compared to a reference volume.

VI. CONCLUSION AND OUTLOOK TO ITER

The selected examples shown for the effects of field line pitch angle aligned resonant magnetic perturbation fields on the electron density and temperature profiles at the last closed flux surface and in the scrape-off layer, including the survey of previously published results, showed that a three-dimensional plasma boundary is induced which transforms the treatment of the plasma wall interaction into a 3D task. A 3D stochastic boundary is induced on both devices, TEXTOR as an example for circular, high field side limited L-mode plasmas and DIII-D with high triangularity, poloidal divertor plasmas including ITER similar shape plasmas at ITER relevant low pedestal electron collisionality. This stochastic boundary consists of stochastic field lines which interact as the interface to the plasma core with intact flux surfaces and a layer of open field lines with short connection length to the divertor targets compared to electron mean free lengths. These so-called laminar field lines are bundled into correlated flux tubes and they form the helical and highly 3D SOL of the stochastic boundary. The analysis approach based on vacuum magnetic field line tracing was validated and we showed that this attempt can describe the newly established topology in the 3D boundary sufficiently for the analysis of the plasma wall interaction in both L- and H-mode plasmas. However, no conclusion is drawn from the target and SOL profile measurements presented, as to what extent the stochastic layer is formed inside of the plasma or how much it is modified or shielded by plasma response effects. The data shown provide on a transport level strong evidence for the fact that at least a thin layer of stochastic field lines must exist which acts as SOL and channels the exhausted fluxes into a helical divertor footprint.

Based on these findings we modelled the magnetic footprint for the latest design of the ITER ELM control coils and the results are presented in Fig. 6. We study two $n = 4$ current distributions with the same nominal RMP current $I_C = 90$ kAt in the coils. The coil configuration found to be most effective in terms of stochastic layer extension with this current, is a square wave distribution along all nine columns of coils [38]. This gives a magnetic flux loss region [26,38], i.e. a region of open field lines with connection to the wall of 0.25 in normalized poloidal flux inward. However, as smooth rotation of the external field is considered for spreading of the localized heat and particle fluxes shown in this contribution for example, we also studied a cosine like distribution of I_C. This current selection reduces the stochastic layer width to 0.16, which still matches the ITER design criterion. The magnetic footprint for the inner strike line is shown in the upper two plots of Fig. 6 and the footprint at the outer strike line is shown in the lower row. The graphs include as a dashed horizontal line the material transition from CFC to Tungsten.

This initial study shows that a similar magnetic footprint pattern evolves as observed during ELM suppression by RMP at DIII-D. We therefore expect non-axisymmetric heat and particle fluxes aligned to this perturbed magnetic topology. For the highly efficient square wave current distribution, the outer tips of the lobes connecting field lines from the deeper interior, reach out to the Tungsten area potentially channelling hot particles or high particle fluxes onto these heat flux sensitive surfaces. In contrast, all lobes stay inside of the CFC domain of the ITER divertor if the perturbation is applied with the cosine wave current distribution. This shows that the coil set currently planned for ITER offers the flexibility needed to fine-tune the eventual heat and particle fluxes during ELM suppression by RMP fields at ITER.

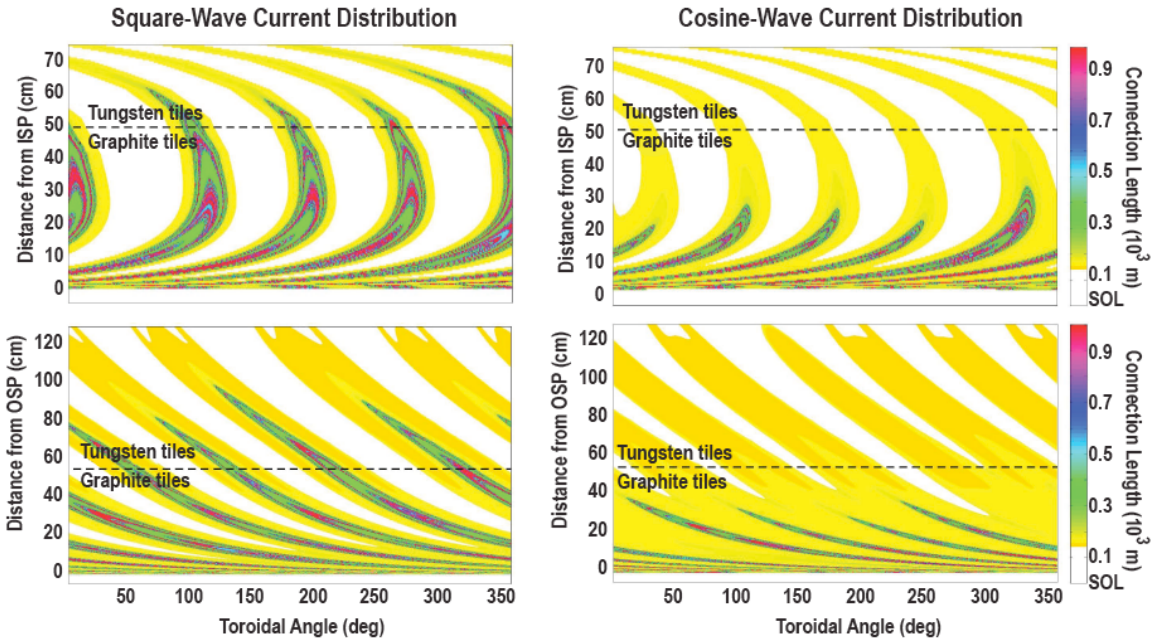

Fig. 6. Magnetic ITER divertor footprint pattern with $n = 4$ RMP spectrum applied with different current distributions to enhance the stochastic layer width. Upper row shows the footprint for at the inner strike line, lower row shows the footprint at the outer strike line. A square wave current distribution with a stochastic layer width of 0.25 in normalized poloidal flux is shown on the left side, and a cosine like current distribution with a reduced stochastic layer width of 0.16 is considered on the right.

REFERENCES

[1] T.E. Evans, *et al.*, Nature Phys. **2**, 419 (2006).

[2] T.E. Evans, *et al.*, Phys. Rev. Letter **92**, 235001-1 (2004).

[3] A. Loarte, *et al.*, Plasma Phys. Control. Fusion **45**, 1594 (2003).

[4] Y. Liang, *et al.*, Plasma Phys. Control. Fusion **49**, B581 (2007).

[5] E. Nardon, *et al.*, Plasma Phys. Control. Fusion **51**, 124010 (2009).

[6] J.M. Cannick, *et al.*, Nucl. Fusion **50**, 034012 (2010).

[7] M. Lehnen, *et al.*, Plasma Phys. Control. Fusion **47**, B237 (2005).

[8] T.N. Todd, *et al.*, Nucl. Fusion **35**, B231-240 (1993).

[9] R.J. Buttery, *et al.*, Nucl. Fusion **36**, 10 (1996).

[10] M. Mori, *et al.*, Plasma Phys. Control. Fusion **35**, B231-240(1993).

[11] Ph. Ghendrih, *et al.*, Nucl. Fusion **42**, 1211 (2002).

[12] O. Neubauer, *et al.*, Fusion Science Techn. **47**, 46 (2005).

[13] J.L. Luxon, *et al.*, Nucl. Fusion **42**, 614 (2002).

[14] T.E. Evans, *et al.*, Nucl. Fusion **48**, 024002 (2008).

[15] M.J. Lanctot, *et al.*, Phys. Plasmas **17**, 056108 (2010).

[16] V. Izzo, *et al.*, Nucl. Fusion **48**, 115004 (2008).

[17] S.S. Abdullaev, *et al.*, Phys. Plasmas **15**, 042508 (2008).

[18] O. Schmitz, *et al.*, Plasma Phys. Control. Fusion **50**, 124029 (2008).

[19] T.E. Evans, *et al.*, "Chaos, Complexity and Transport: Theory and Applications," World Scientific, Singapore, (ed C. Chandre) (2008).

[20] O. Schmitz, *et al.*, Nucl. Fusion **48**, 024009 (2008).

[21] A. Wingen, *et al.*, Nucl. Fusion **49**, 055027 (2009).

[22] M. Kobayashi, *et al.*, Phys. Plasmas **17**, 056111 (2010).

[23] Y. Feng, *et al.*, Nucl. Fusion **45**, 89-95 (2005).

[24] M. Jakubowski, *et al.*, J. Nucl. Mater. **363-365**, 671 (2007).

[25] T.E. Evans, *et al.*, J. Phys. Conf. Series **7**, 174 (2005).

[26] O. Schmitz, *et al.*, Phys. Rev. Lett. **103**, 165005-1 (2009).

[27] H. Frerichs, *et al.*, Nucl. Fusion **50**, 034004 (2010).

[28] M. Jakubowski, *et al.*, Phys. Ref. Letter **96**, 035004 (2006).

[29] O. Schmitz, *et al.*, J. Nucl. Mater. **363-365**, 680 (2007).

[30] H. Stoschus, *et al.*, Phys. Plasmas (2010), accepted for publication.

[31] T.E. Evans, *et al.*, J. Nucl. Mater. **363-365**, 570 (2007).

[32] E. Nardon, *et al.*, these proceedings, P1-43.

[33] P. Cahyna, *et al.*, these proceedings, P1-41.

[34] A.G. McLean, *et al.*, Rev. Scientific Inst. **80**, 043501 (2009).

[35] A.G. McLean, *et al.*, J. Nucl. Mater. **390-391**, 160-163 (2009).

[36] S. Brezinsek, *et al.*, J. Nucl. Mater. **363-365**, 1119-1128 (2007).

[37] J. Roth, *et al.*, Nucl. Fusion **44**, L21-L25 (2004).

[38] D. Orlov, *et al.*, EPS conference 2010, Dublin, Ireland.

ACKNOWLEDGMENTS

This work was supported in part by the U.S. Department of Energy under DE-FC02-04ER54698, DE-FG02-07ER54917, DE-AC52-07NA27344, DE-FG02-89ER53297, DE-AC05-00OR22725, and DE-AC04-94AL85000.